Numerical investigation of an airfoil with a Gurney flap

Cory S. Jang[a], James C. Ross[b], Russell M. Cummings[a]

[a] *California Polytechnic State University, San Luis Obispo, CA 93407, USA*
[b] *NASA Ames Research Center, Moffett Field, CA 94035, USA*

Abstract

A two-dimensional numerical investigation was performed to determine the effect of a Gurney flap on a NACA 4412 airfoil. A Gurney flap is a flat plate on the order of 1–3% of the airfoil chord in length, oriented perpendicular to the chord line and located on the airfoil windward side at the trailing edge. The flowfield around the airfoil was numerically predicted using INS2D, an incompressible Navier–Stokes solver, and the one-equation turbulence model of Baldwin and Barth. Gurney flap sizes of 0.5%, 1.0%, 1.25%, 1.5%, 2.0%, and 3.0% of the airfoil chord were studied. Computational results were compared with available experimental results. The numerical solutions show that some Gurney flaps increase the airfoil lift coefficient with only a slight increase in drag coefficient. Use of a 1.5% chord length Gurney flap increases the airfoil lift coefficient by $\Delta C_l \approx 0.3$ and decreases the angle of attack required to obtain a given lift coefficient by $\Delta \alpha_{L=0} > -3°$. The numerical solutions show the details of the flow structure at the trailing edge and provide a possible explanation for the increased aerodynamic performance.

Nomenclature

c	airfoil reference chord	e, f	inviscid flux terms in x, y directions, respectively
C_d	sectional drag coefficient ($= d/q_\infty c$)	e_v, f_v	viscous flux terms in x, y directions, respectively
C_f	total skin friction coefficient	L	geometric length scale
C_l	sectional lift coefficient ($= l/q_\infty c$)	l	sectional lift
C_m	sectional pitching moment coefficient (taken about $c/4$) ($= m/q_\infty c^2$)	m	sectional pitching moment coefficient
d	sectional drag	p	pressure
		q_∞	freestream dynamic pressure ($= \frac{1}{2}\rho U_\infty^2$)

Re	Reynolds number ($= U_\infty c/\upsilon$)	α	angle of attack
t	physical time	β	artificial compressibility factor
u, v	velocity components in x, y directions, respectively	υ	kinematic viscosity
		ρ	density
U_t	friction velocity, $U_\infty \sqrt{C_f/2}$	τ	pseudo-time parameter
U_∞	freestream velocity	τ_{ij}	stress tensor
x, y	spatial dimensions in physical plane	∞	freestream conditions
y^+	wall dimension, yU_t/υ		

1. Introduction

The high-lift performance of a commercial aircraft has a large influence on the economic viability of that aircraft. An effective high-lift system allows greater payload capacity for a given wing, as well as a longer range for a given gross weight. The generation of increased lift also allows for a steeper takeoff ascent, which can reduce the amount of noise imparted to the area surrounding an airport. An increase in the climb lift-to-drag ratio makes it possible for the aircraft to attain cruise altitude faster, resulting in a more fuel-efficient flight. Finally, mechanically simple high-lift systems would minimize manufacturing and maintenance costs, and therefore increase an aircraft's profitability.

One mechanically simple way to increase the lift coefficient of an airfoil is by using the Gurney flap. Liebeck stated that race car testing by Dan Gurney showed that the vehicle had increased cornering and straight-away speeds when the flap was installed on the rear wing [1]. The increased cornering speeds were attributed to the increased downforce (i.e. lift) applied by the inverted wing. It was also noticed, however, that increasing the flap size above 2% of the wing chord length noticeably increased the drag, even though there was a continuing increase in downward force. Liebeck tested a 1.25% chord Gurney flap on a Newman airfoil and found that the lift coefficient was increased with a small decrease in the drag coefficient. Liebeck hypothesized that the Gurney flap effectively changed the flowfield in the region of the trailing edge by introducing two contrarotating vortices aft of the flap, which altered the Kutta condition and circulation in the region (see Fig. 1). He based his assumption on the trailing edge flowfield for a clean airfoil reported by Kuchemann [2]. When Liebeck used a tufted probe in the vicinity of the trailing edge he noticed considerable turning of the flow over the back side of the flap.

A wind tunnel investigation of the Gurney flap was also conducted on a multi-element race car wing by Katz and Largman [3], and on a four element car wing by Katz and Dykstra [4]. In both investigations the wings tested used end plates to structurally fix the elements in place, as well as to increase the lift-curve slope by reducing three-dimensional affects. The Gurney flaps were located on the trailing edge of the most aft wing element in both studies. Katz and Largman reported that using a 5% chord Gurney flap increased the lift coefficient of the wing above the baseline wing by about 50% [3]. However, the drag increased to such an extent that the lift-to-drag ratio was decreased in the design angle of attack range of the wing ($2° \leq \alpha \leq 12°$). Katz and Dykstra found that adding a 2% chord Gurney flap increased the wing lift coefficient as well as the drag coefficient [4]. Wing lift-to-drag ratio with the Gurney flap was also lower than the baseline wing in this study.
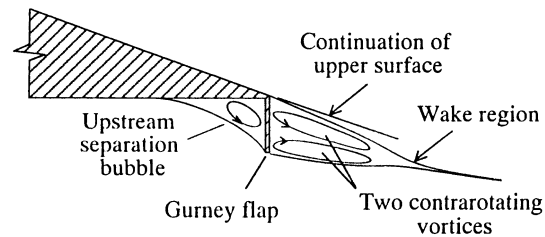
Fig. 1. Hypothesized trailing edge flow structure for an airfoil with a Gurney flap (from description in [1]).

Roesch and Vuillet reported on an Aerospatiale wind tunnel test involving the use of the Gurney flap on the horizontal tails and vertical fins of various helicopter models [5]. Gurney flap sizes of 1.25% and 5% chord length were examined on the horizontal stabilizer, which used a NACA 5414 airfoil section. The results showed that the 5% chord Gurney flap increased the lift coefficient by 40%, raised the lift curve slope by 6%, and shifted the angle of attack for zero lift by $\Delta\alpha_{L=0} = -6°$. The drag polars, however, indicated that larger Gurney flap sizes caused an increase in drag coefficient at moderate and low values of lift coefficient. For the case of the 5% chord flap, the drag coefficient was almost doubled at moderate lift coefficients. However, while the lift improvement was less with the 1.25% chord flap, there was no significant drag penalty. While the drag reduction benefits hypothesized by Liebeck were not seen in the Aerospatiale tests, Roesch and Vuillet reported general agreement between the two studies.

A water tunnel study of several Gurney flap configurations was performed on a NACA 0012 wing by Neuhart and Pendergraft [6]. Flow visualization results showed that Liebeck's hypothesized flowfield caused by the Gurney flap was generally correct, and that the effect of the Gurney flap was to increase the local camber of the trailing edge. This hypothesis was strengthened by the results of Sewall et al., whose wind tunnel tests studied the effects of increasing the local trailing edge camber of the EA-6B wing [7]. The lift curve was shifted upwards from the baseline geometry, which gave higher maximum lift as well as a more negative $\alpha_{L=0}$. Just as with the 1.25% chord Gurney flap, there was no appreciable drag penalty associated with the trailing edge modifications at low and moderate lift coefficients.

The computed effects of the Gurney flap in the current study (as well as in [5]) are very similar to the pressure, lift, and drag changes that occurred with the use of the Divergent Trailing Edge (DTE) device reported by Hemme [8]. The modified trailing edges used in that study were very much like a Gurney flap, with the high pressure side filled in with a concave ramp. Hemme stated that the DTE acted like a Gurney flap on a high-speed airfoil.

The objective of the present study is to provide quantitative and qualitative computational data on the performance of the Gurney flap. Computations of a baseline NACA 4412 airfoil are compared with experimental results obtained in a two-dimensional wind tunnel test performed at the NASA Ames 7- by 10-foot Wind Tunnel by Wadcock [9]. Subsequent computations were performed to determine the effect of various sizes of Gurney flaps on the lift and the drag of the same airfoil.

2. Theoretical background

Governing Equations. The non-dimensional Reynolds-averaged Navier–Stokes equations for incompressible viscous flow written in two dimensions may be expressed as

$$\frac{\partial \tilde{u}}{\partial \tilde{x}} + \frac{\partial \tilde{v}}{\partial \tilde{y}} = 0 \, , \tag{1}$$

$$\frac{\partial \tilde{u}}{\partial \tilde{t}} + \frac{\partial}{\partial \tilde{x}} \left(e - e_{\mathrm{v}} \right) + \frac{\partial}{\partial \tilde{y}} \left(f - f_{\mathrm{v}} \right) = 0 \, , \tag{2}$$

where $\tilde{x}_i = x_i/L$, $\tilde{t} = t\,U_\infty/L$, $\tilde{u}_i = u_i/U_\infty$, $\tilde{p} = p/\rho U_\infty^2$, $\tilde{v} = v/LU_\infty = \mathrm{Re}^{-1}$, and $\tilde{\tau}_{ij} = \tau_{ij}/\rho U_\infty^2$. Details about the non-dimensionalization and the flux vectors, $e, e_{\mathrm{v}}, f, f_{\mathrm{v}}$, can be found in [10, 11].

To enhance convergence of numerical solutions of these equations, the concept of artificial compressibility can be applied by adding a time derivative of pressure to the continuity equation (1):

$$\frac{\partial \tilde{p}}{\partial \tau} = -\beta \nabla \cdot \tilde{u} \, , \tag{3}$$

where β is the artificial compressibility parameter and τ a pseudo-time parameter [10]. Together, the momentum and modified continuity equations form a hyperbolic system of partial differential equations which can be solved with various compressible flow algorithms. As these equations are marched through pseudo-time, $\partial \tilde{p}/\partial \tau \to 0$, and the artificial compressibility term drops out.

Turbulence model. The present study assumes that the flow over the airfoil surface is completely turbulent. This matches the wind tunnel test conditions, which used a grit boundary-layer trip near the leading edge of the airfoil. Turbulence viscosity is determined using the Baldwin–Barth turbulence model, an eddy-viscosity model that combines the transport equations of turbulent kinetic energy and turbulence dissipation into one equation [12]. Flows over various airfoils have been computed using the model without the need to calculate a turbulence length scale, which makes it more desirable for flows with confluent shear/boundary layers and wakes [12].

Numerical algorithm. The implicit numerical scheme employed is the INS2D algorithm as reported by Rogers and Kwak in [10] and Rogers in [12]. The algorithm uses flux-difference splitting to allow upwind differencing of the convective terms. The upwind differencing yields a natural numerical dissipation without the need for added artificial dissipation. The equations are solved using an implicit line-relaxation scheme, which provides a stable way for iterating with large pseudo-time step values, and allows for faster convergence.

3. Geometry modeling and grid generation

Geometry modeling. The geometry used for the Gurney flap study is a NACA 4412 airfoil. Computations were performed for Gurney flap sizes ranging from 0.5% to 3% chord length, with the flaps located on the windward side of the airfoil at the trailing edge. For simplicity, the wind tunnel walls used for the experiment were not modeled. INS2D has the capability to select points in the computational grid where solutions will be obtained. Any interior surface can be created within

the computational mesh by "blanking out" the appropriate rows and/or columns of points to describe the surface. A no-slip boundary condition is then specified on the "blanked out" points to create the viscous walls on the Gurney flap. This feature was used to test various sizes of Gurney flaps while using only one grid.

Grid generation. All of the computations were performed using a 250×69 C-grid as shown in Fig. 2. The top and bottom farfield boundaries are six chord lengths from the airfoil; the upstream and downstream boundaries are five and seven chord lengths away, respectively. The grid was constructed using the grid generation code Gridgen2D [13]. The algebraic stretching function of Vinokur was used to determine the point distribution circumferential, and normal, to the airfoil surface [14]. This allowed for the modeling of various sizes of Gurney flaps, which were nominally situated perpendicular to the airfoil chordline. Transfinite interpolation was then used to determine the point distribution for the interior points.

Fig. 3 shows a closer view of the grid in the vicinity of the airfoil. Grid clustering is evident near the surface of the airfoil, as well as near the trailing edge, to obtain reasonable resolution of the boundary layer and the region around the Gurney flap. The first grid point above the surface is located at $y^+ \approx 1$. Fig. 4 shows a grid with a 1.25% Gurney flap at the airfoil trailing edge, as modeled by the "blanked out" region.

4. Results and discussion

Computations were performed for a NACA 4412 airfoil at conditions which match the experimental data of Wadcock [9]. The Reynolds number for the computational cases matches the experimental Reynolds number, based on wing chord, of $Re_c = 1.64 \times 10^6$. The wind tunnel test
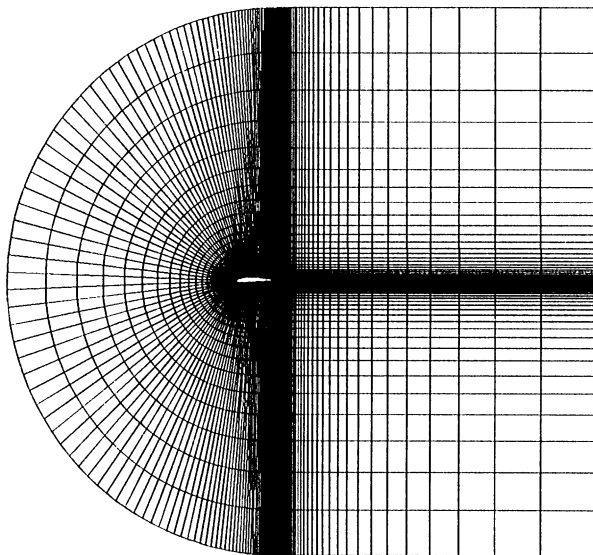

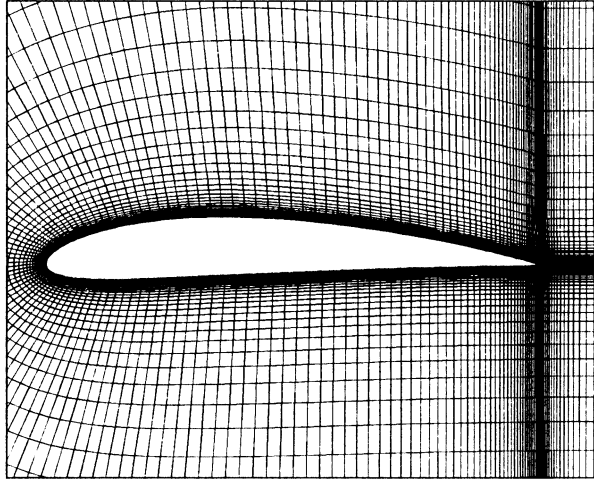Fig. 2. 250×69 C-grid used in computations.

Fig. 3. Closeup of grid showing clustering near the surface of the airfoil and at the trailing edge.
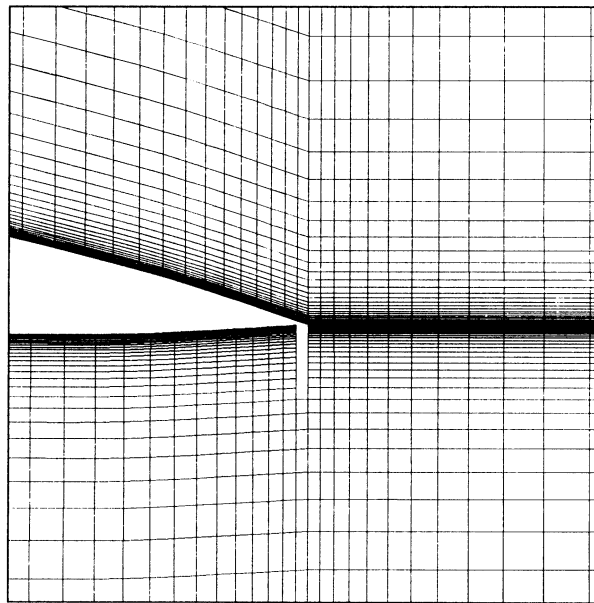

Fig. 4. Details of grid in the vicinity of the trailing edge, including the blanked-out grid points which form the Gurney flap.

was performed at the NASA Ames Research Center 7- by 10-foot Wind Tunnel at a Mach number of 0.085. Force measurements were taken for $0° \leq \alpha \leq 18°$, with surface pressures measured at discrete angles of attack up to $\alpha = 10°$.

Code validation. Experimental results are compared with computations for the baseline airfoil in Fig. 5 (no Gurney flap simulation). The two-dimensional computations are compared with tunnel centerline data from the two-dimensional wing, which spanned the wind tunnel. The computations
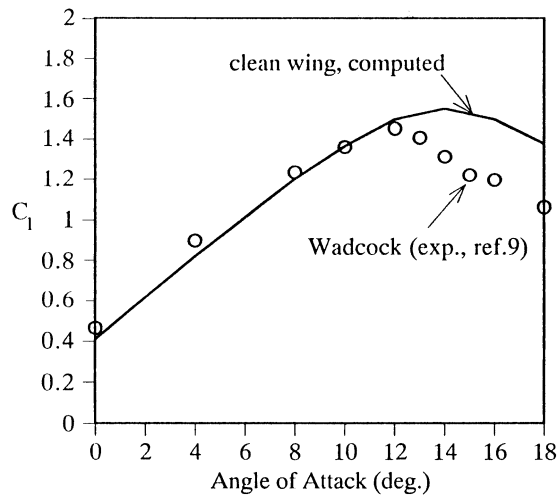
Fig. 5. Comparison of computed lift coefficients with experimental data; NACA 4412 airfoil, $Re_c = 1.64 \times 10^6$.
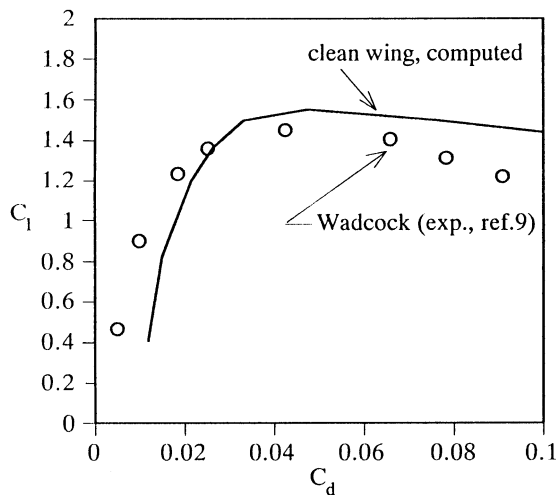

Fig. 6. Drag polar comparison; NACA 4412 airfoil, $Re_c = 1.64 \times 10^6$.

agree well with the measured data up to $\alpha \approx 12°$. While this is the point of maximum lift for the NACA 4412 airfoil ($C_{l_{max}} = 1.45$), the INS2D code with the Baldwin–Barth turbulence model predicts that the maximum lift coefficient occurs at $\alpha = 14°$ ($C_{l_{max}} = 1.55$). Since the Gurney flaps will be simulated at angles of attack below stall, this comparison shows that the Navier–Stokes predictions are simulating the pre-stall flowfield quite well.

Fig. 6 shows comparisons between experimental and computational drag polars. While there is general agreement with the experimental data, there are differences between the two results. The computed flowfield has more separation than the experiment for $\alpha < 13°$ (Fig. 7), which may account for the computed drag being higher than the experimental values at the lower lift

coefficients. The experimental results exhibit more flow separation for $\alpha > 13°$, and the predictions more closely match the data.

The disparity of flow separation locations may be due to a variety of factors. The computations in this study do not take into account any wall blockage that may have occurred in the wind tunnel test. Also, the comparison of the fully turbulent solutions with data where the flowfield is mostly, but not completely, turbulent (due to trip strips near the airfoil leading edge) can cause differences in results. In addition, the one-equation turbulence model is applied at non-flat-plate conditions, which can also cause discrepancies.

A typical comparison between the computed pressure distribution and measured data at $\alpha = 8°$ can be seen in Fig. 8. Favorable agreement between the predictions and data can be seen at all
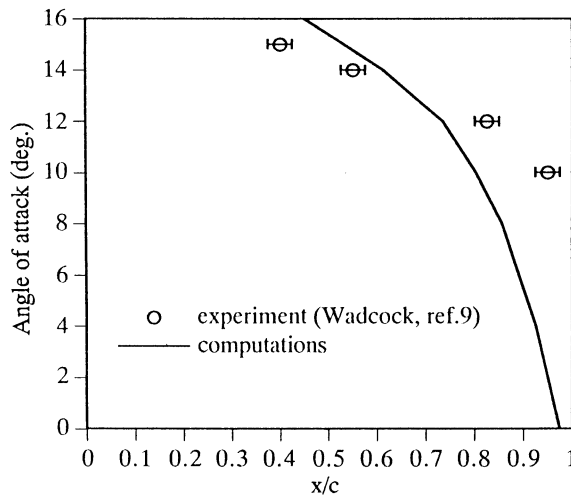
Fig. 7. Upper surface separation locations; NACA 4412 airfoil, $Re_c = 1.64 \times 10^6$.
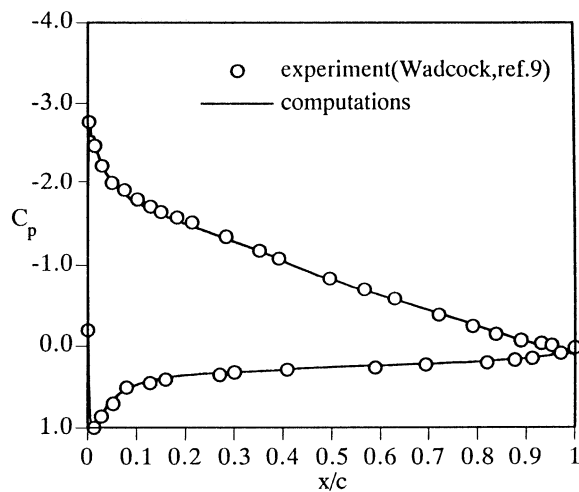
Fig. 8. Surface pressure coefficient distributions; NACA 4412 airfoil, $\alpha = 8°$, $Re_c = 1.64 \times 10^6$.

locations on the upper and lower surfaces of the airfoil. More detailed validation of the numerical method applied to the Gurney flap may be found in [15, 16].

Lift, drag, and pitching moment. Fig. 9 shows the computed results for the NACA 4412 airfoil with different size Gurney flaps. In general, the lift coefficient increases as the Gurney flap size increases for a given angle of attack. As an example, a 1.25% chord Gurney flap shifts the lift curve by more than 3°, but the relationship between the Gurney flap size and lift-curve shift does not appear to be linear. Specifically, the increase in lift coefficient due to changing the Gurney flap size from 0% to 0.5% chord is greater than the change found by changing the flap from 2% to 3% chord. Fig. 10 shows how Gurney flap height affects both the lift and pitching moment coefficients at $\alpha = 0°$. There is an increase in nose-down pitching moment as the Gurney flap becomes larger,
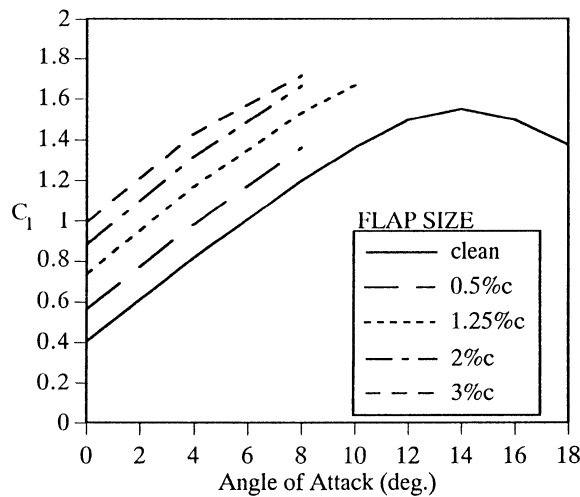
Fig. 9. Effect of Gurney flap size on lift coefficient; NACA 4412 airfoil, $Re_c = 1.64 \times 10^6$.
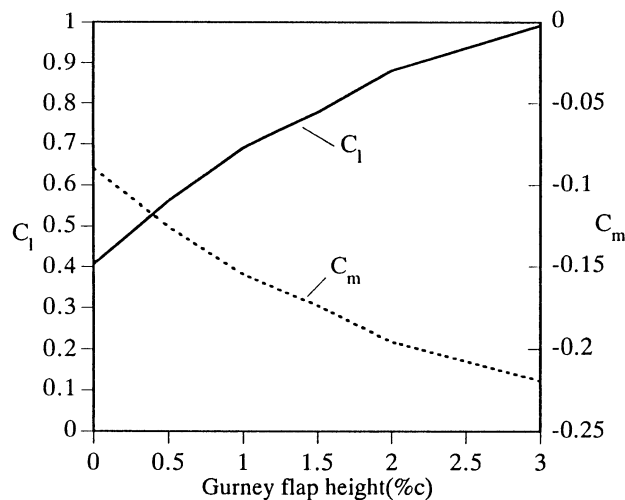
Fig. 10. Effect of Gurney flap size on lift and pitching moment coefficients; NACA 4412 airfoil, $Re_c = 1.64 \times 10^6$.

but the moment increment becomes less with increasing Gurney flap size. Nevertheless, the nose-down pitching moment coefficient is more than doubled for the 3% chord flap case compared with the baseline airfoil.

The effect of Gurney flap size on the drag coefficient can be seen in Fig. 11. The addition of the flap increases the drag coefficient at low and moderate levels of lift coefficient. However, flap sizes less than 1.25% chord results in a very small increase in drag. An added benefit of the Gurney flap on the NACA 4412 airfoil is an increase in the lift-to-drag ratio for $C_1 > 1.4$.

Separation and pressure distribution. The effect of the Gurney flap on the upper surface separation location is of particular interest. The movement of the upper surface separation point as the Gurney flap size is increased is shown in Fig. 12. At $\alpha = 4°$ the addition of a 0.5% chord Gurney
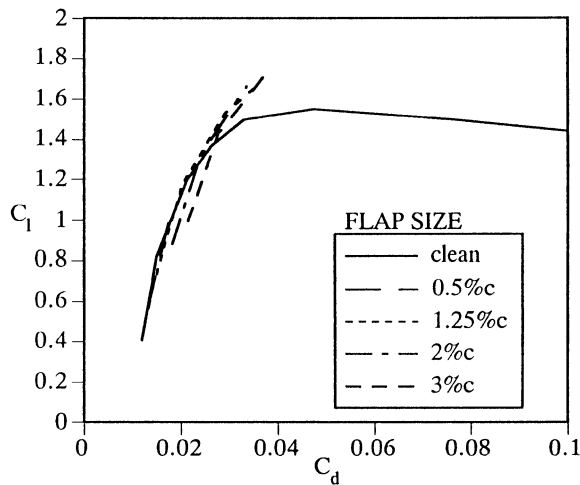
Fig. 11. Effect of Gurney flap size on drag polars; NACA 4412 airfoil, $Re_c = 1.64 \times 10^6$.
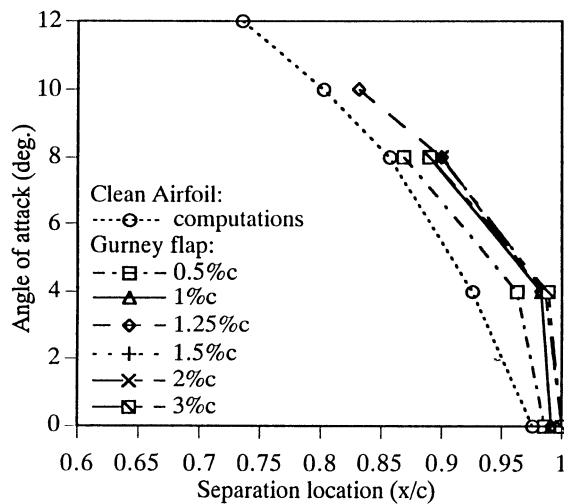
Fig. 12. Effect of Gurney flap size on upper surface separation location; NACA 4412 airfoil, $Re_c = 1.64 \times 10^6$.

flap moves the onset of separation location aft by approximately 4% compared to the clean airfoil case. Flaps larger than 1% chord further shift the separation point to approximately the 99% chord location. At $\alpha = 8°$, the 0.5%, 1%, and 1.25% chord flaps also move the upper surface separation point downstream (as also took place at $\alpha = 4°$). However, Gurney flap sizes larger than approximately 1.25% chord yield no further shifting of the point of separation. In fact, the 3% chord flap moves the separation location slightly upstream of the 0.5% chord flap separation location.

The effect of the Gurney flap on airfoil pressure distribution at various angles of attack is shown in Fig. 13a–d. The flap increases the pressure difference between the upper and lower surfaces,
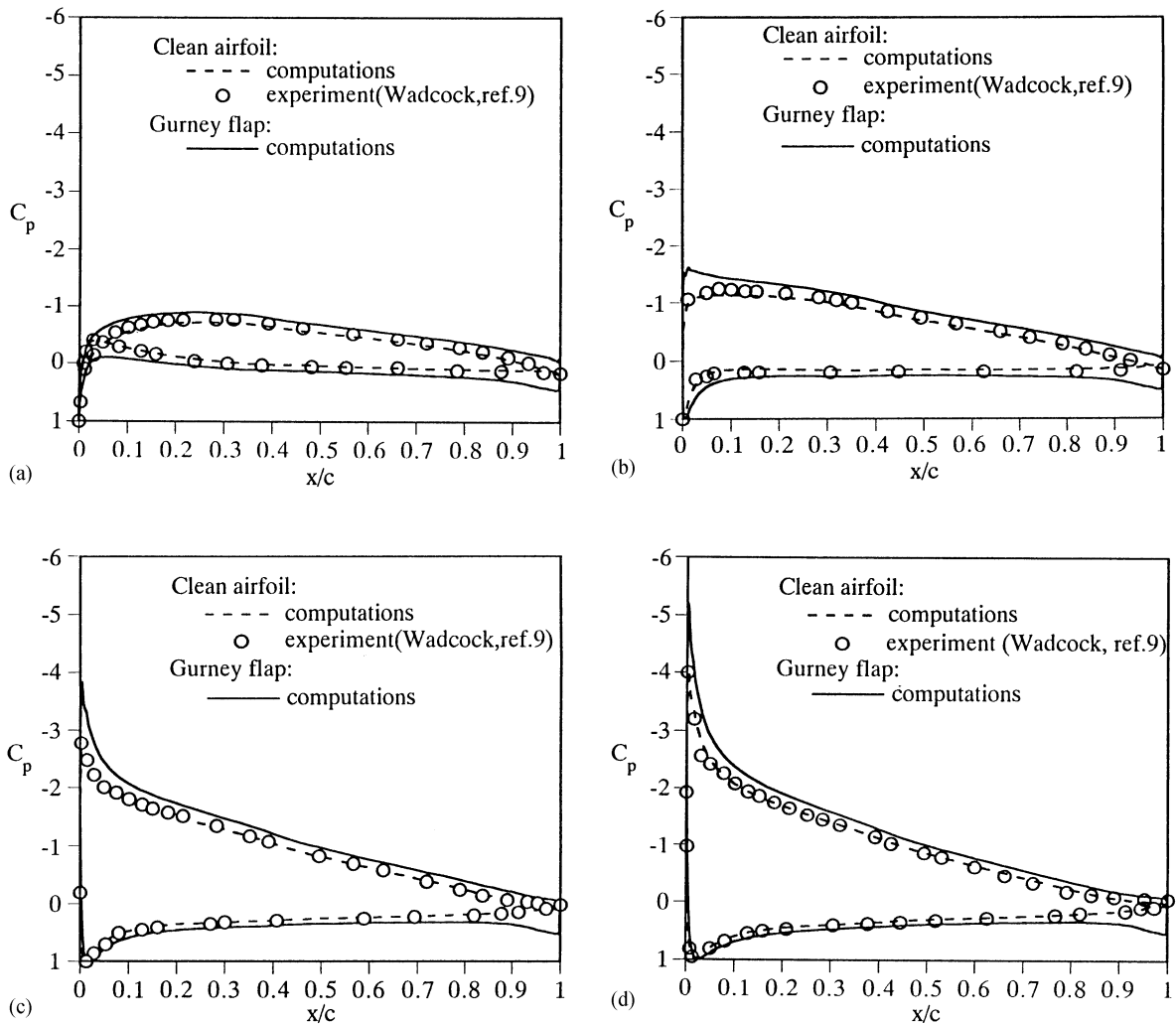

Fig. 13. Surface pressure coefficient distribution for a 1.25% chord Gurney flap; NACA 4412 airfoil, $Re_c = 1.64 \times 10^6$. (a) $\alpha = 0°$; (b) $\alpha = 4°$; (c) $\alpha = 8°$; (d) $\alpha = 10°$.

particularly in the vicinity of the trailing edge. This leads to increased lift and additional nose-down pitching moment. The increase in trailing edge loading was also observed in the experimental pressure distributions for an advanced technology airfoil with a 1.25% chord Gurney flap, as reported by Neuhart and Pendergraft [6]. Fig. 14 shows that as the Gurney flap size increases (for a given angle of attack) the pressure difference between the upper and lower surfaces of the airfoil becomes larger. The loading along the entire airfoil is increased, particularly at the suction peak and near the Gurney flap.

Trailing edge flow structure. Fig. 15 shows the computed flowfield in the vicinity of the airfoil trailing edge for $\alpha = 8°$ with and without a 1.25% chord Gurney flap. A recirculation region can be seen in front of the flap and a strong clockwise vortex is apparent on the upper backside of the flap. However, no easily discernable contrarotating vortex can be seen in the region behind the Gurney flap, as was hypothesized in [1]. The separation region on the suction side of the airfoil with the Gurney flap is much smaller than on the clean wing. In addition, the particle traces show increased downwash behind the flapped airfoil, which indicates that increased lift is being generated by the Gurney flap.

The flow mechanism that makes the Gurney flap work so effectively is its effect on the trailing-edge Kutta condition. The low pressure region behind the Gurney flap causes a downward momentum of fluid in the region above the trailing edge. The suction side of the airfoil has increased velocity as well as a smaller upper-surface recirculation region, which results in increased lift. This smaller separation region on the suction side of the airfoil also has the benefit of counteracting the drag caused by the Gurney flap itself. The flap has a positive pressure coefficient on the windward side and a negative pressure coefficient on the leeward side, resulting in a net drag on the flap. The flow turning caused by the Gurney flap is similar to an increase in the camber at the airfoil trailing edge, as reported by Neuhart and Pendergraft [6]. Computations using the Gurney flap also show trends similar to the results of Sewall et al. [7], who increased the local trailing edge camber of a wing.
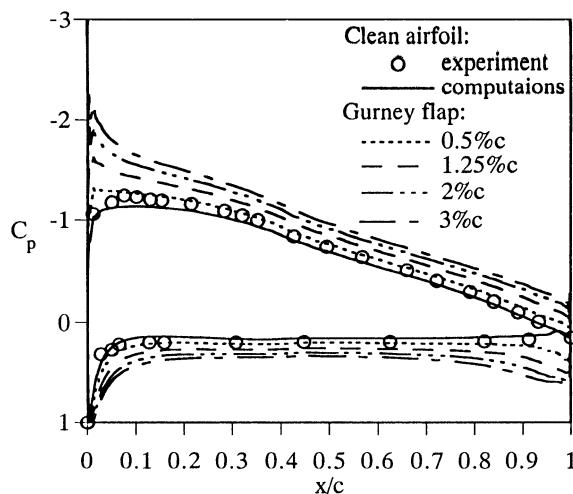

Fig. 14. Effect of Gurney flap size on surface pressure coefficient distribution; NACA 4412 airfoil, $Re_c = 1.64 \times 10^6$, $\alpha = 4°$.
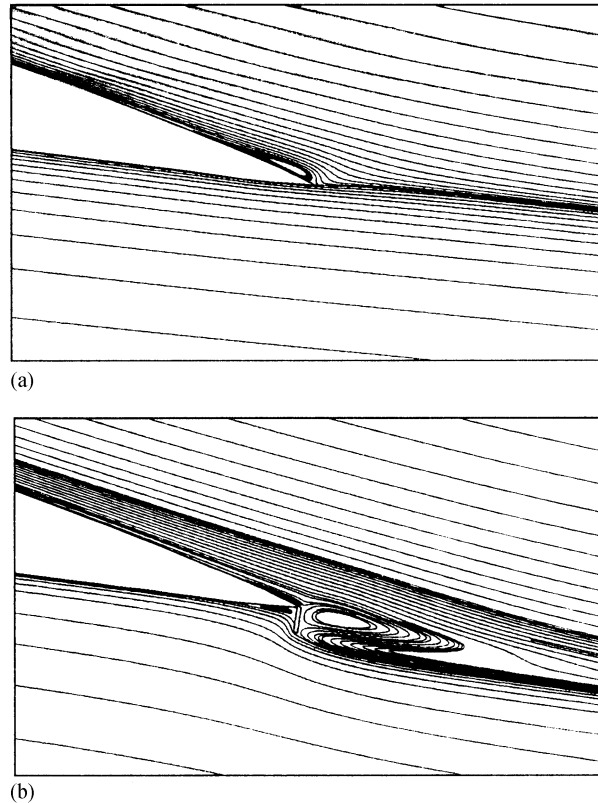
(a)

(b)

Fig. 15. Computed particle traces in the vicinity of the NACA 4412 airfoil; $Re_c = 1.64 \times 10^6$, $\alpha = 8°$. (a) Airfoil with no Gurney flap and (b) Airfoil with 1.25% chord Gurney flap.

5. Conclusions

A computational study of the flowfield for a NACA 4412 airfoil with a Gurney flap has been completed. The two-dimensional flow was calculated using the INS2D code with the one-equation turbulence model of Baldwin and Barth. The trends observed in the two-dimensional computations were found to agree well with available experimental results. While not all hypothesized flow features were captured in the wake downstream of the Gurney flap, enough of the flow disturbances caused by the application of the Gurney flap were captured to obtain results consistent with experimental data.

In comparison with a clean airfoil, lift coefficient and nose-down pitching moment were increased by the Gurney flaps. However, larger Gurney flaps will increase lift at the expense of increasing drag. Gurney flap sizes less than 1.25% of the main airfoil chord will result in an increased lift coefficient, with very little increase in drag. In fact, at higher lift coefficients the drag is lower than that of the clean airfoil configuration. The separation point of the NACA 4412 airfoil with a Gurney flap is farther aft at moderate angles of attack than that of a clean airfoil. Also, the

use of the Gurney flap increases the loading along the entire length of the airfoil, with a large increase in trailing-edge loading.

The Gurney flap is an intriguing device for high-lift design because of the mechanical simplicity of the device and the significant impact on aerodynamic performance. Subsonic aircraft could greatly benefit from the use of this simple flat-plate device.

Acknowledgements

References

[1] Liebeck RH. Design of subsonic airfoils for high lift. Journal of Aircraft 1978;15(9):547–61.
[2] Kuchemann D. Inviscid shear flow near the trailing edge of an airfoil. Z. Flugwiss, 1967;15:292–4.
[3] Katz J, Largman R. Effect of 90 degree flap on the aerodynamics of a two element airfoil. Journal of Fluids Engineering 1989;111:93–4.
[4] Katz J, Dykstra L. Study of an open-wheel racing car's rear-wing aerodynamics. SAE Paper 890600, March 1989.
[5] Roesch P, Vuillet A. New designs for improved aerodynamic stability on recent Aerospatiale helicopters. Vertica 1982;6:145–64.
[6] Neuhart DH, Pendergraft OC. A water tunnel study of Gurney flaps. NASA TM 4071, November 1988.
[7] Sewell WG, McPhee RJ, Ferris JC. Wind tunnel test results of airfoil modifications for the EA-6B. AIAA Paper 87-2359, August 1987.
[8] Hemme PA. Innovation with computational aerodynamics: the divergent trailing edge airfoil. Applied Computational Aerodynamics. New York: AIAA, 1990, 221–61.
[9] Wadcock AJ. Investigations of low-speed turbulent separated flow around airfoils. NASA CR 177450, August 1987.
[10] Rogers SE, Kwak D. An upwind differencing scheme for the time-accurate incompressible Navier–Stokes equations. AIAA Paper 88-2583, June 1988.
[11] Rogers SE. Numerical solution of the incompressible Navier–Stokes equations. NASA TM 102199, November 1990.
[12] Baldwin BS, Barth TJ. A one-equation turbulence transport model for high Reynolds number wall-bounded flows. AIAA Paper 91-610, January 1991.
[13] Steinbrenner JP, Chawner JR, Fouts CL. The GRIDGEN 3D multiple block grid generation system. WRDC-TR-90-3022, July 1990.
[14] Vinokur M. On one-dimensional stretching functions for finite difference calculations. NASA CR 3313, 1980.
[15] Jang CS. Incompressible Navier–Stokes computations of an airfoil with a Gurney flap. M.S. Thesis, California Polytechnic State University, 1992.
[16] Jang CS, Ross JC, Cummings RM. Computational evaluation of an airfoil with a Gurney flap. AIAA Paper 92-2708, June 1992.